PERFORMANCE OF SUBGRID FLAMELET MODEL IN LES OF REACTING, TURBULENT FLOWS

XIAODAN CAI AND FOLUSO LADEINDE
Aerospace Research Corporation, L.I.
P.O. Box 1527
Stony Brook, NY 11790-0609

Abstract. Large eddy simulation (LES) with a flamelet-based chemistry model has been evaluated through *a priori* and *a posteriori* tests in both decaying homogeneous turbulence and spatially-developing mixing layers. The present flamelet-LES approach involves a series of models, among which are the models for the PDF of mixture-fraction ($f(z)$) and the conditional filtered dissipation rate ($\widetilde{\chi}_{st}$). We test three models for $f(z)$: a) $\delta-$PDF ($f(z) = \delta\left(\widetilde{Z}\right)$), b) $\beta-$PDF, c) Gaussian PDF; and two models for $\widetilde{\chi}_{st}$. The Gaussian PDF model consistently performs almost as well as the $\beta-$PDF, and may provide an alternative approach to the $\beta-$PDF method. This point is important to the LES simulations since the calculation of Gaussian function is much cheaper than that of $\beta-$function. Furthermore, it may be said from the error analyses that the counterflow model for $\widetilde{\chi}_{st}$ has average performance in its present form and that a phenomenological model in the form of Eq. (6) exists with an optimum value of a parameter C_3 to produce a better result. The *a posteriori analysis* shows a satisfactory performance of the flamelet model within the context presented in this paper.

1. Introduction

Large eddy simulation (LES) constitutes an attractive approach for numerical simulation of turbulent reacting flows. The basic idea of LES is to calculate the large-scale energy-containing eddies and use a subgrid model for the small scales. The large-scale structures resolved by LES are effective entrainers and play a role in bringing various reactive gas pockets into contact before the reactants are mixed by molecular diffusion, prior to reaction. Hence, the entrainment rates induced by the large-scale structures will

determine the overall reaction rates in a turbulent reacting flow, and are sometimes crucial to the understanding of flame behavior, especially when combustion instabilities occur[1]. LES is thus regarded as a favorable tool in combustion applications, better than the traditional Reynolds-Averaged Navier-Stokes (RANS) turbulent models which are limited to the description of the mean flow field.

However, relatively few studies have addressed LES of reacting flows. Modeling subgrid combustion activities encounters great challenges. Unlike the aerodynamic problem, the use of the similarity assumption for the small-scale mixing and dissipation processes in reactions leads to unresolved terms which are related to the heat release. In addition, a more serious problem for LES combustion models is that the chemical reactions almost always take place within the unresolved subgrid scales. For example, an approximate model neglecting subgrid scale contributions, i.e., writing the reaction rates as an Arrhenius law in terms of the filtered quantities, significantly misrepresents the combustion dynamics[2]. The modeling tasks are then as challenging as in RANS applications.

The current practice in modeling the subgrid combustion activities generally follows the concepts and the techniques once developed for RANS applications. They include the direct methods, such as the extended version of the Eddy-Break-Up model[2], the Linear-Eddy model[3], the Transported Probability Density Function (TPDF) method[4] and the Conserved Scalar method, such as the flamelet approach[5]. Some new models based on the similarity concept have also been suggested[6]. Until recently, the focus was on *a priori* testing of the applicability of combustion models in LES[7]; the evaluation of the models by *a posteriori* testing is not as common, except in the studies of Menon and his co-workers[8] and Pitsch and Steiner[9].

The basic procedure for the flamelet-LES model used in the present paper is contained in Cook and Riley[7]. However, the present paper uses this technique within the framework of a generalized curvilinear coordinate system to permit the calculation of turbulent combustion in realistic systems which usually have complex geometries. The main contribution of the present paper is in the investigation of the various model assumptions used for the calculation of the mixture-fraction dissipation rate and its PDF. Both the *a priori* and *a posteriori* testing through direct numerical simulation (DNS) and LES of turbulent non-premixed flames are reported.

2. Subgrid Flamelet Models

The generalized curvilinear coordinate formulation for the large-eddy simulation follows Jordan[11], where the full Navier-Stokes equations are transformed prior to filtering. The filtered reaction rate is approximated by the

laminar flamelet model. That is, in the unresolved subgrid scales, combustion takes place in a thin layer in the vicinity of the surface of stoichiometric mixture fraction where its local gradient is sufficiently high. Therefore, the combustion in a turbulent flow is represented by a statistical ensemble of such laminar flamelets. At each grid point, the filtered reaction rate is therefore modeled as

$$\overline{\dot{\omega}_i}(\mathbf{x}) = \iint \dot{\omega}_i(Da, Ze, Ce, P_0, Y_{i1}, Y_{i2}, T_1, T_2; Z, \chi_s) \cdot f(Z, \chi_s; \mathbf{x})\, dZ d\chi_s. \tag{1(a)}$$

The mass fraction is also modeled in a similar fashion:

$$\overline{Y_i}(\mathbf{x}) = \iint Y_i(Da, Ze, Ce, P_0, Y_{i1}, Y_{i2}, T_1, T_2; Z, \chi_s) \cdot f(Z, \chi_s; \mathbf{x})\, dZ d\chi_s. \tag{1(b)}$$

In the above equations, $\dot{\omega}_i$ and Y_i are the reaction rates and species mass fractions obtained from the steady-state laminar flamelet calculations[5]. The input to the flamelet calculations includes the free-stream values of species concentrations (Y_{i1}, Y_{i2}) and temperatures (T_1, T_2), and the stoichiometric dissipation rates, which have to be modeled from the LES calculations. The normalized parameters Da, Ze and Ce are, respectively, the Damkhöler number, Zeldovich number, and the Heat Release parameter.

The joint probability density function of the mixture fraction and its dissipation rate, $f(Z, \chi_s)$, contains the statistical information on the flamelets in a turbulent flow. Statistical independence is assumed for the mixture fraction (Z) and its scalar dissipation rate (χ_s):

$$f(Z, \chi_s; \mathbf{x}) = f(Z; \mathbf{x}) \cdot f(\chi_s; \mathbf{x}).$$

As most reactions occur around the flame sheet, which is close to the stoichiometric surface in a statistical sense, it is reasonable to assume that

$$f(\chi_s; \mathbf{x}) = \delta(\widetilde{\chi}_{\mathbf{st}}), \tag{2}$$

and $f(Z; \mathbf{x})$ is usually modeled by the β–form PDF:

$$f(Z; \mathbf{x}) = \frac{Z^{a-1}(1-Z)^{b-1}}{B(a,b)}, \tag{3}$$

where $a = \widetilde{Z} \cdot \left[\frac{\widetilde{Z}(1-\widetilde{Z})}{<Z''^2>} - 1\right]$, $b = a(\frac{1}{\widetilde{Z}} - 1)$, and $B(a,b) = \frac{\Gamma(a+b)}{\Gamma(a)+\Gamma(b)}$. This paper compares the performance of β–form PDF model with that of a Gaussian PDF:

$$f(Z; \mathbf{x}) = \left(\frac{1}{2\pi < Z''^2 >}\right)^{1/2} \exp\left(-\frac{\left(Z - \widetilde{Z}\right)^2}{2 < Z''^2 >}\right). \tag{4}$$

Similarity assumption[7] has been used to model the filtered mixture fraction variance and dissipation rate for the *a posteriori* test which, respectively, are

$$\widetilde{Z''^2} = \widetilde{Z^2} - \tilde{Z}^2 \simeq C_1 \left[\widehat{(\tilde{Z})^2} - \left(\hat{\tilde{Z}} \right)^2 \right],$$

and

$$\tilde{\chi} \simeq C_2 \cdot D \frac{\partial \tilde{Z}}{\partial x_i} \frac{\partial \tilde{Z}}{\partial x_i}.$$

The symbol "$\hat{}$" implies test-level filtering. The constants $C_1 \simeq 1.3$ and $C_2 \simeq 1.1$ have been chosen from direct numerical simulations that were carried out as part of the present study. For the *a priori* test, they are obtained directly from the DNS data. Cook and Riley[7] proposed the use of the counterflow assumption to close the conditional filtered dissipation rate ($\tilde{\chi}_{st}$) with the above filtered dissipation rate, i.e.,

$$\tilde{\chi}_{st} \simeq \tilde{\chi} \frac{\exp\left\{-2\left[erfc^{-1}(2Z_{st})\right]^2\right\}}{\int_0^1 \exp\left\{-2\left[erfc^{-1}(2Z)\right]^2\right\} f(Z)dZ}. \tag{5}$$

However, it is argued that the counterflow structure is rarely found in realistic turbulent reacting flows. For example, recent DNS of turbulent, reacting mixing layers[22] found that the chemical reaction occurs typically in a shear-type stretching mode instead of a counterflow structure, even though the concept of laminar flamelets was still applicable in this case. A mapping-closure approach has been attempted by the current authors[23] to replace the counterflow model. However, little improvement has been found. One phenomenological model that has been used in RANS modeling is evaluated in this paper but within the framework of the flamelet-LES procedure being reported on. The phenomenological model takes the form

$$\tilde{\chi}_{st} \simeq C_3 \tilde{\chi}. \tag{6}$$

3. Numerical Procedures

Both DNS and LES are performed to evaluate the subgrid models through *a priori* and *a posteriori* testings. The numerical methods employed to solve the DNS/LES equations are the compact schemes for the spatial derivatives and the classical fourth-order Runge-Kutta scheme for the time integration. This is combined with a high-order filtering procedure[10] in order to suppress numerical instabilities arising from the unsolved scales, mesh non-uniformities and boundary conditions. It must be noted that this filtering

operation has a much weaker attenuation effect on the Fourier amplitudes of ϕ_i than the LES filters so that this effect won't mask the the effect of the LES filter. The LES filter scheme uses the Simpson's averaging scheme. To account for the boundary effects, the Navier-Stokes Characteristic Boundary Condition (NSCBC)[14] is extended to the generalized curvilinear coordinate system in the present work. The steady flamelet equations are solved by the Newton-Raphson method, as described in Ladeinde *et al*[15].

A single-step, irreversible chemical reaction of the type

$$F + rO \longrightarrow (r+1)\,P, \tag{7}$$

is used, where r represents the mass stoichiometric ratio of oxidizer to fuel, and is related to the stochiometric value of mixture-fraction by $Z_{st} = [1 + r \cdot Y_{F,1}/Y_O]^{-1}$. For methane/air combustion, which is represented by Case 2, $r = 4$ and $Z_{st} = 0.055$. The reaction rate assumes the form

$$\dot{\omega}_r = \rho^2 \cdot Da \cdot Y_1 Y_2 \cdot \exp\left(-\frac{Ze}{T}\right).$$

The two-dimensional calculations in this work are able to capture the essential features of the reaction mechanism. The test cases are listed in Table 1. Case 1 and Case 2 involve decaying homogeneous turbulence with initial Reynolds number of $Re_0 = 250$. The initial field for Z is random with a pseudo double-delta probability distribution[17]. The initial fields for the mass fractions of the reacting species are then generated from Z assuming the fast-limit reaction. The smallest turbulent scales under the Reynolds number of 250 are fully resolved by the DNS grids for Case 1 and Case 2. Case 3 involves a spatially-developing mixing layer with an inflow Reynolds number of 720 (based on vorticity thickness). The convective Mach number is 0.125 with a ratio of slow- to fast-stream velocity 0.5. Both the initial velocity field and the initial mixture-fraction field use the hyperbolic tangent profile, and the initial mass fraction fields for the reacting species are generated from Z, assuming the fast-limit reaction distribution. The inflow conditions are generated by superposition of small perturbations on the mean field. To facilitate the formation of roll-up structures, the perturbations are generated from the fundamental modes ($\omega_0 = 1.3198$) obtained from linear-stability analysis[24]. The DNS grids for Case 3 have a resolution of 25η (η is the Kolmogorov length scale), which seems fine enough for the mixing layer turbulent flows[20] when the large-scale structures dominate the flow behaviors. LES was carried out for Case 1 and Case 3 but not for Case 2. However, Case 2 was used in the evaluation of the flamelet model (Figure 1).

Table 1. Test Cases.

Test	Flow Type	Z_{st}	Da	Ze	Ce	DNS Grid	LES Grid
Case 1	Homogeneous	0.5	10	0	0	133×133	35×35
Case 2	Homogeneous	0.055	10	0	0	133×133	N/A
Case 3	Mixing Layer	0.5	10	5	1.0	375×99	186×49

4. Evaluation of Models

Flamelet Calculation: Prior to the *a priori* and *a posteriori* analyses of model performance, flamelet calculations are carried out to obtain the values of $\dot{\omega}_i$ and Y_i for the integrals in Eq. (1). The calculations are performed in the mixture-fraction space[15]. Note that the parameters Da, Ze and Ce, are required for the flamelet calculations. The values of $\dot{\omega}_i$ and Y_i from the flamelet calculation are then constructed in the form of a look-up table (indexed by $\widetilde{Z}, < Z''^2 >, \tilde{\chi}$) to facilitate the LES calculations. Figure 1 shows the product mass fraction results from the flamelet calculations for Case 1 and Case 2. The effects of conditional scalar dissipation rate on species distribution appear to be significant for the chemistry model in Eq. (7), especially around the stoichiometric values of the mixture-fraction. This result implies that the scalar dissipation rate model has significant effects on the filtered reaction rates and filtered mass fractions of product around their maximum values, which occur close to the stoichiometric value in mixture fraction space. However, it is noted that the same chemistry model has been used by DesJardin and Frankel[6] but with the erroneous assumption that the concentrations of the species were independent of the scalar dissipation rate.

a priori analysis: Data sets from the DNS for the three cases are used to evaluate the accuracy of the flamelet models. To proceed with the analysis, the DNS data is filtered by the Simpson's scheme onto coarse grid-points ($\Delta_{DNS} = C \cdot \Delta_c$, where Δ_{DNS} is DNS grid-spacing and Δ_c is the coarse-grid spacing). The "exact" values for $\overline{Y_p}$, $\overline{\dot{\omega}_f}$, $\widetilde{Z}$, $\widetilde{Z''^2}$ and $\tilde{\chi}$ are used to represent their corresponding filtered quantities on the coarse grid point. The last three quantities are then used to obtain the model values for $\overline{Y_p}$ and $\overline{\dot{\omega}_f}$ using the flamelet model described above. Since the grid-coarsening factor, C, determines the number of sampled DNS points in each LES grid point, it may affect the statistical properties of the embedded flamelets. Therefore, we test two levels of this parameter: $C = 2$ and $C = 4$.

Figure 2 shows the contour maps of product mass-fraction obtained from DNS for Case 1 (eddy-turn-over time of 4.0, Figure 2(a)) and Case 3

(evolution time of 208, Figure 2(b)). The contour maps evidently show that the fine flow-structures are suitably resolved, and therefore can be used to evaluate the flamelet chemistry model.

It is noted that the present flamelet-LES approach involves a series of models, among which are the models for the PDF of mixture-fraction ($f(z)$) and the conditional filtered dissipation rate ($\widetilde{\chi}_{st}$). We test three models for $f(z)$: a) $\delta-$PDF ($f(z) = \delta\left(\widetilde{Z}\right)$, b) $\beta-$PDF (Eq. 3), c) Gaussian PDF (Eq. 4); and two models for $\widetilde{\chi}_{st}$ (Eq. 5 and Eq. 6). The errors from these models have been evaluated by two criteria, $\sum \frac{(X_{model}-X_{exact})^2}{X_{exact}^2}$ and $\sum \frac{(X_{model}-X_{exact})^2}{(X_{exact}^2)_{\max}}$, where X represents $\overline{Y_p}$ or $\overline{\dot{\omega}_f}$. As Criterium 2 puts more weight on the large values, it is considered to be more suitable for evaluating the model performance in the sense that the model has more significant effects on the behaviors of $\overline{Y_p}$ and $\overline{\dot{\omega}_f}$ around their maximum values, which are discussed at the beginning of this section. Figures 3(a), 3(b), and 3(c) present the model errors for $\overline{\dot{\omega}_f}$ for Cases 1, 2 and 3, respectively, with grid-coarsening factor $C = 2$. Figure 3(d) shows the model errors for $\overline{\dot{\omega}_f}$ with $C = 4$ (Case 1). The values of C_3 for the counterflow model in the figures represent an averaged quantity over the whole domain since the counterflow model for $\widetilde{\chi}_{st}$ produces a local C_3 value at each grid point. From these figures we see that the errors for the Gaussian PDF model and the $\beta-$PDF are much smaller than those for $\delta-$PDF. The improvement in the Gaussian PDF and $\beta-$PDF prediction increases with increasing values of C. Since the use of $\delta-$PDF implies that there is no local PDF model for the mixture fraction on each LES grid point, the improvement in the Gaussian PDF and $\beta-$PDF predictions suggests that the use of some subgrid PDF models, even though simple, will be very helpful in LES calculations, a point consistent with the results obtained by Jimenez *et al.*[21] It is also observed that the Gaussian PDF model consistently performs almost as well as the $\beta-$PDF, although the latter is used more often in the literature. The results here suggest that the use of the Gaussian PDF is equally acceptable. This point is important since the Gaussian function is much cheaper to calculate than the β function. Furthermore, it can be seen from Figure 3 that the $\widetilde{\chi}_{st}$ model also has a strong effect in comparison to the Gaussian and $\beta-$PDF models. The graphs clearly show that an optimal C_3 value exists for each case. It may be said that the performance of the counterflow model is modest in comparison to the performance of the phenomenological models in Eq. (6). This point is strengthened by Figure 4, which shows the correlation between the exact and modeled values of $\overline{\dot{\omega}_f}$ in the form of scatter plots for the three cases. Here, the results from the counterflow model for $\widetilde{\chi}_{st}$ are compared with those from Eq. (6) using the optimal value of coefficient C_3.

a posteriori analysis: The *a posteriori* tests are considered to be the

ultimate tests of model performance in the sense that the model is evaluated only after it has been implemented in the large-eddy simulation. Figure 5(a) shows the correlation between the DNS and LES values of $\overline{Y_p}$ (Case 1) in the form of scatter plots. It appears from this figure that the LES-flamelet procedure, along with the assumptions in Eq. (3) and Eq. (6), is capable of generating accurate results. Further evidence comes from a comparison of the growth rates of momentum thickness θ in the DNS and the LES-flamelet calculations for the spatially-developing mixing layers (Figure 5(b)). The LES-flamelet model gives better results compared to those without the model. However, owing to the combined effects of numerical discretization in space and time, and averaging[13], *a posteriori* tests of the mixing layer flows do show some scatter for the correlation between the DNS and LES values of $\overline{Y_p}$.

5. Conclusions

We have shown satisfatory performance of a flamelet-LES procedure for decaying homogeneous turbulence and the spatially-developing mixing layer. The chemical reaction used in the tests has a moderate Damkhöler number and a reasonable Zeldovich number but with weak heat release. The laminar-flame structures of the chemical reactions are strongly dependent on the conditional scalar dissipation-rate and are thus very sensitive to the model for this quantity.

We use the *a priori analysis* to compare the model values of $\overline{Y_p}$ and $\overline{\dot{\omega}_f}$ with their corresponding "exact" values from DNS data sets. The error analyses prove that the use of some subgrid models for the PDF of mixture-fraction, even though simple, yields accurate LES calculations, which is consistent with the observations of Jimenez *et al.*[21] We also see in this study that the Gaussian PDF model consistently shows a comparable performance to the more common $\beta-$PDF, and may provide an alternative approach. This point is important because the Gaussian function is much cheaper to calculate than the β function. Furthermore, it may be said from the error analysis that the counterflow model shows only a moderate performance

The *a posteriori analysis* confirms the observation that the performance of the flamelet-LES procedure consistent with the model assumptions in this paper appears to be satisfactory. However, owing to the combined effects of numerical discretization in space and time, and averaging, *a posteriori* tests of the mixing layer flows show some scatter for the correlation between the DNS and LES values of $\overline{Y_p}$.

References

1. 1. McManus, K.R., Poinsot, T. and Candel, S., *Progress in Energy and Combustion Science*, Vol. 19, p.1-29 (1993).
2. 2. Candel, S., Thevenin, D., Darabiha, N., and Veynante, D., *Combust. Sci. and Tech.*, Vol.149, pp. 297-337 (1999)
3. 3. Kerstein, A.R., *Combust. Sci. and Tech.*, Vol.60, pp.391 (1988)
4. 4. Gao, F. and O'Brien, E. E., *Phys. Fluids* A, 5, pp. 1282-1284, (1993)
5. 5. Peters, N., *Prog. Energy Combust. Sci.*, Vol. **10,** p. 319-339 (1984).
6. 6. DesJardin, P.E. and Frankel, S.H., *Phys. Fluids* Vol. 10(9), pp.2298-2314 (1999).
7. 7. Cook, A. W. and Riley, J. J. *Combustion and Flame* 112:593, (1998).
8. 8. Chakravarthy, V.K. and Menon, S. In "Recent Advances in DNS and LES", (D. Knight and L. Sakell, Eds.), Kluwer Academic Publishers, pp. 85-98 (1999).
9. 9. Pitsch, H. and Steiner, H., *Phys. Fluids* Vol. 12(10), pp.2541-2554 (2000).
10. 10. Visbal, M.R. and Gaitonde, D.V., AIAA Paper 98-0131, January 199108.
11. 11. Jordan, S.A., *J. Comp. Phys.* Vol.148, pp.322-40 (1999).
12. 12. Janicka, J. and Peters, N., *19th Symposium (international) on Combustion*, the Combustion Institute, Pittsburg, pp. 367-374 (1982).
13. 13. Meneveau, C. and Katz, J., *Annu. Rev. Fluid Mech.* 32:1-32 (2000).
14. 14. Poinsot, T.J. and Lele, S.K., *J. Comp. Phys.* **101**, pp.104-129 (1992).
15. 15. Ladeinde, F., Cai, X. and Sekar, B. paper 2000-GT-144, IGTI Congress and Exhibition, Munich, Germany (2000).
16. 16. Ladeinde, F., O'Brien, E.E., Cai, X., Liu, W., *Phys. Fluids* **8** (11) (1995) 2848-2857.
17. 17. Mell, W.E., Nilsen, V., Kosaly, G. and Riley, J.J., *Phys. Fluids* **6** (3) (1994), 1331-1356.
18. 18. Piomelli U, Moin P, and Ferziger JH, *Phys. Fluids* **31** (A) (1988), 1884-1891.
19. 19. Ribault, C.L., Sarkar, S. and Stanley, S.A., *Phys. Fluids* **11** (10) (1999) 3069-3083.
20. 20. Freund, J.B., Moin, P. and Lele, S., Department of Mechanical Engineering, Stanford University, Report No. TF-72.
21. 21. Jimenez, J., Linan, A., Rogers, M. and Higuera, F., *J. Fluid Mech.* (1997), vol.349, pp.149-171.
22. 22. Miller, R.S., Madnia, C.K. and Givi, P. "Structure of a turbulent reacting mixing layer," Comb. Sci. and Tech. (1994) Vol. 99(3), 1.
23. 23. Cai, X.D., Ladeinde, F. and Sekar, B. "Some issues in the use of laminar flamelet model in LES", Bulletin of the American Physics Society, Vol. 44 (8), P.45, 1999.
24. 24. Michalke, A., "On the invisid instability of the hyperbolic-tangent velocity profile", *J. Fluid Mech.* **19**, 543-56 (1964).

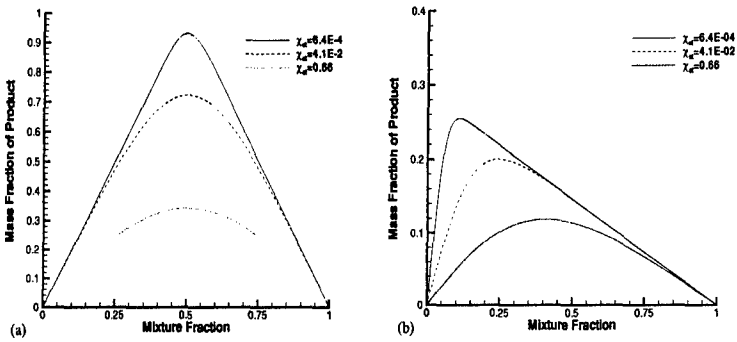

Figure 1. Flamelet results for Case 1 (a) and Case 2 (b), showing the effects of different values of χ_{st}

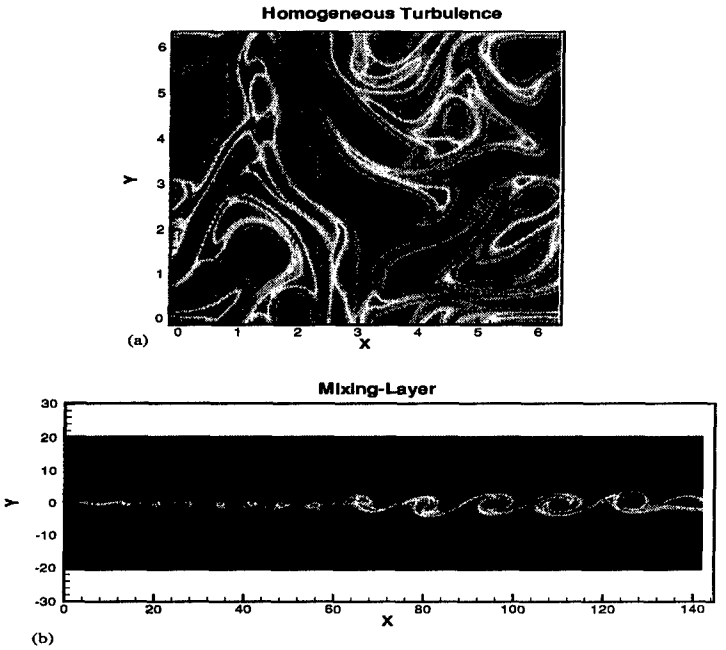

Figure 2. Contour maps of product mass-fraction at time of: a) $t = 4.0$ (Case 1); b) $t = 208$ (Case 3).

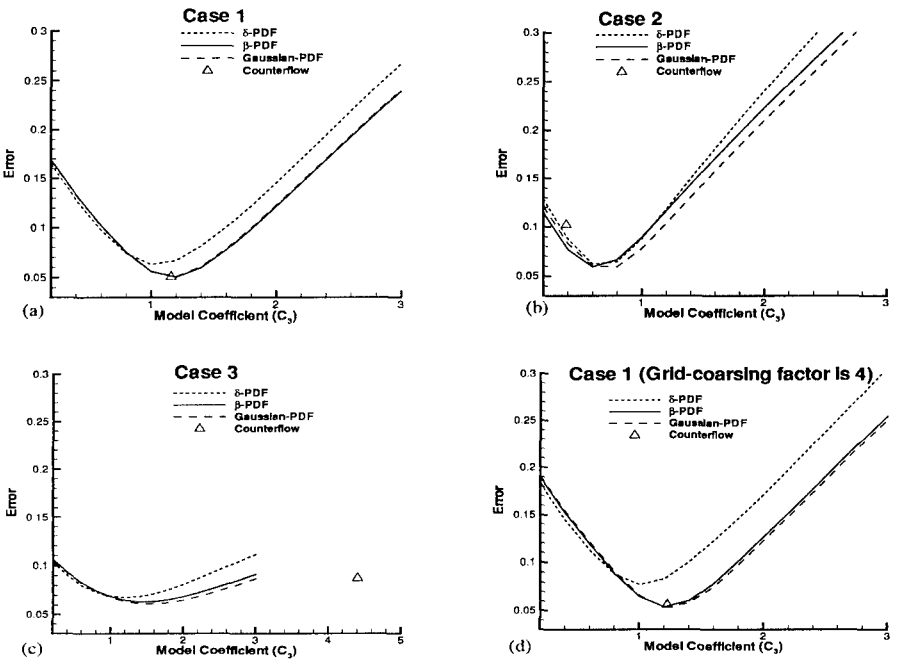

Figure 3. The effect of Coefficient C_3 on the model errors of $\overline{\dot{\omega}_f}$ for the three cases ((a)-(c)), with $C = 2$. The error plot in Figure 3(d) is for Case 1 with $C = 4$.

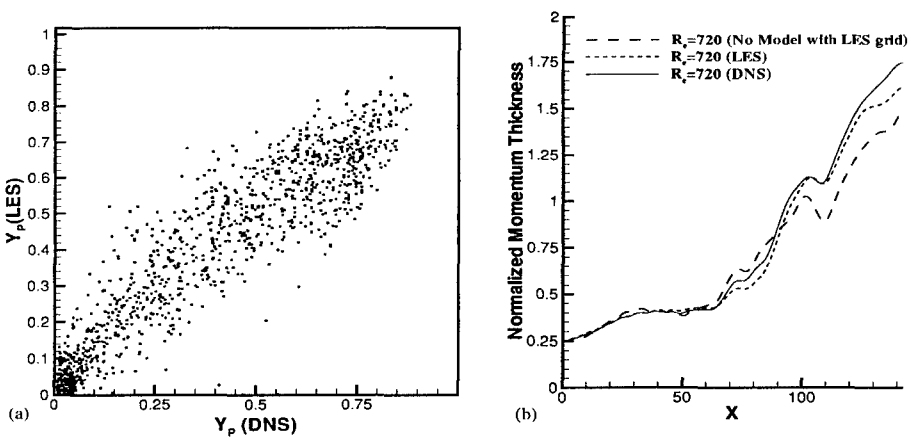

Figure 5. *a posteriori* tests of model performance: a) the correlation between DNS and LES values of $\overline{Y_p}$ in the form of scatter plots for Case I; b) comparison of the growth rates of the momentum thickness θ from DNS and flamelet-LES calculations.

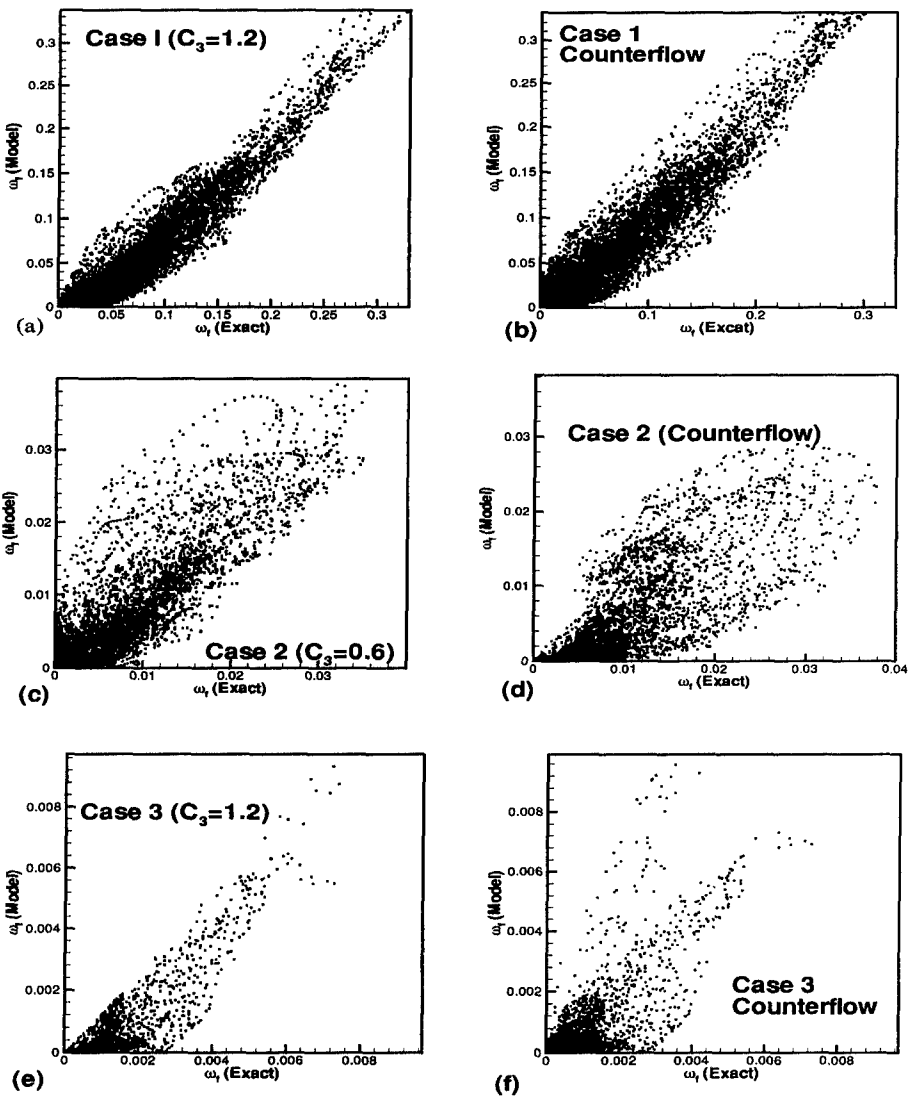

Figure 4. The correlation between the exact and modeled values of $\overline{\dot{\omega}_f}$ in the form of scatter plots. Figure 4(a), (c), and (e) use Eq. (6) with the values of C_3 as shown while Figure 4(b), (d), and (f) use the Counterflow model for $\widetilde{\chi}_{st}$.